

Dynamic wrinkling and strengthening of a filament in a viscous fluid

Julien Chopin*

*Sciences et Ingénierie de la Matière Molle, CNRS UMR 7615, ESPCI Paris,
PSL Research University, 10 rue Vauquelin, F-75231 Paris cedex 05, France and
SIMM, UPMC Univ Paris 06, Sorbonne-Universités,
10 rue Vauquelin, F-75231 Paris cedex 05, France*

Moumita Dasgupta and Arshad Kudrolli

Department of Physics, Clark University, Worcester, Massachusetts 01610, USA

(Dated: May 10, 2022)

Slender structures embedded in complex fluids which buckle and fold as a result of mechanical compression are commonly found as in F-actin and microtubules in cell mechanics [1–4], flagella in swimming organisms [5–7], fibers in paper processing [8], and the earth’s crust in orogenesis [9]. While buckling typically occurs in the fundamental mode corresponding to the lowest strain, higher modes can occur depending on the constraints along the filament which may be static or dynamic [10–13]. We develop a model to analyze the loading rate dependent growth of wrinkling modes and relaxation of an elastic filament immersed in a viscous fluid and to go beyond the stationary Euler limit. The fluid drag results in a dynamic lateral reinforcement of the filament leading to wave numbers which increase with power $1/6$ as a function of loading rate during compression followed by a decay to the fundamental mode. We discover the emergence of a new timescale for the mode growth that explicitly depends on the loading rate and corresponds to the crossover time from the extensible to the inextensible regime. When the loading rate is slower than the growth rate, we find that the wrinkling amplitude grows exponentially as the square of the loading rate and cubically with time in contrast with increasing exponentially with time as in the sudden loading limit.

Traditional approaches to the wrinkling observed in elastic filaments consider linear stability analysis with instantaneous loading which can be an oversimplification in many situations [3, 4, 14, 15]. For example, the buckling of membranes, the motion of living systems or actuated membrane involves the change of distance between material points in response to a stimuli (stress, light, pH, temperature) whose dynamics is set externally [16–24]. Additionally, in-plane and out-of-plane modes experience dynamics with a timescale highly dependent on the surrounding environment as in air [25], intra-cellular medium [26], or a viscous fluid [27]. In this context, the interplay between the dynamics of an external stimuli and the dynamics of the elastic modes have been largely

overlooked. Here, we examine a model system that reveals the emergence of a new timescale for the growth of wrinkles that explicitly depends on the loading rate. The precise understanding of this interplay is important for the development of fast reacting thin structures and the tuning of the rheological response of polymers.

Experiments were performed with an elastic filament clamped at both ends and immersed in a container filled with a viscous fluid. The filament has a length $L = 92$ mm, width $W = 3.0$ mm and thickness $h = 0.30$ mm and is composed of vinylpolysiloxane with a Young’s modulus $E = 1$ MPa, and Poisson’s ratio $\nu \approx 0.5$. The bending and stretching moduli are given by $B = Eh^3W/12$ and $K = EhW$ respectively. An anisotropic filament cross section was chosen to have a well defined plane in which the filament buckles, simplifying data acquisition and analysis. One clamped end of the filament is attached to a motorized translating stage which can be moved through a displacement u which varies between $u_0 < 0$ when the filament is under tension, and $u_f > 0$ when the filament is under compression with speed V_e in the range 5×10^{-3} mm/s – 10 mm/s. The fluid composed of a glycerol-water mixture is prepared so that the filament is neutrally buoyant and has a dynamic viscosity $\eta = 0.9$ Pa.s at 25°C. The viscous drag coefficient is given by $\mu \approx 4\pi\nu/\log(L/W)$ [28, 29]. Unless otherwise stated, distances and time are normalized by L and $\tau = \mu L^2/K = 3 \times 10^{-2}$ s. With this rescaling, the non-dimensional speed $V = \tau V_e/L$ ranges between 2×10^{-6} and 3×10^{-3} .

The filament is imaged with a 1200×1200 pixel camera at 1500 fps by placing a diffused light source on the opposite side of the container which allows a good contrast for subsequent image analysis. We then obtain the filament deflection w to within $0.15h$ as a function of the non-dimensionalized coordinate along the longitudinal direction x and time t . We calculate the bending content $\kappa(t) = h^2 \langle (\nabla^2 w(x, t))^2 \rangle$, where $\langle \dots \rangle$ denotes average over the length of the filament, and the averaged strain normalized by L given by

$$\gamma(t) = -u(t) + 1/2 \int_0^1 \nabla w(x, t)^2 dx, \quad (1)$$

where ∇ stands for the partial derivative with respect to

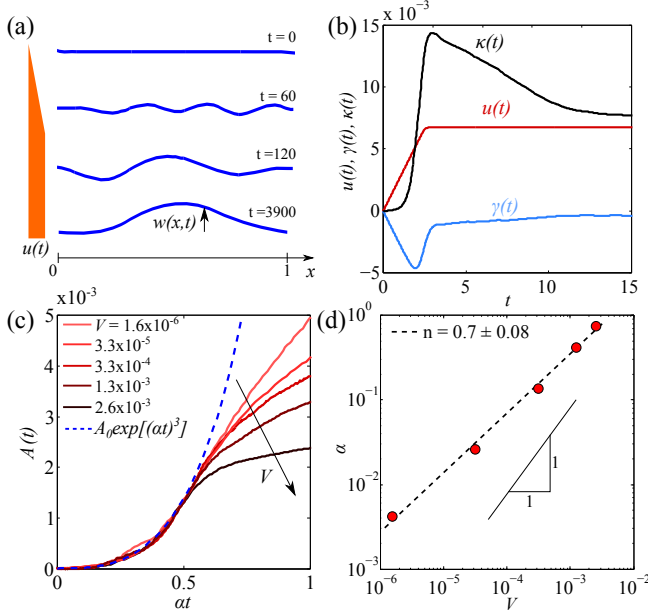


FIG. 1. (a) Snapshots of the measured filament deflection $w(x,t)$ at various times t with the applied strain as a function of time illustrated by the bar on the left ($u_f = 7 \times 10^{-3}$). Wrinkles emerge during loading followed by coarsening till the fundamental buckling mode is reached. (b) The measured strain γ is observed to relax rapidly while the ribbon is being compressed. In contrast, the bending content $\kappa(t)$ associated with the coarsening dynamics relaxes much slower while the ends of the filament are held with a prescribed strain. (c) The initial evolution of $A(t)$ for various V is observed to collapse on to a single curve using a fitting parameter α . (d) α is observed to scale sub-linearly as a function of V with an exponent $n = 0.7 \pm 0.08$.

x . This expression is obtained by integrating the 1D non-linear strain $\gamma(x,t) = \nabla u(x,t) + 1/2(\nabla w(x,t))^2$, where $u(x,t)$ is the local in-plane axial displacement [30]. The evolution of the stretching and bending energies stored in the filament can be then quantified by $\gamma(t)$ and $\kappa(t)$, respectively.

Fig. 1(a) shows the measured profile at various times while the filament is loaded as denoted by the bar on the left. The filament is observed to undergo a wrinkling instability during the loading phase ($t < t_f = u_f/V$) with a wavelength which is approximately a third of the length of the ribbon. Shortly thereafter, the ribbon is observed to undergo spontaneous coarsening till the wavelength reaches the filament length, and the shape corresponds to the fundamental buckling mode calculated using time-independent Euler analysis [31]. We obtain the evolution of γ and the bending content κ , and plot $u(t)$, $\gamma(t)$, and $\kappa(t)$ in Fig. 1(b) focusing on a time interval over which most of the initial buckling and coarsening occurs. At the onset of instability, $\gamma(t)$ and $\kappa(t)$ are observed to increase rapidly showing the increase of the bending energy and the relaxation of the compression. From the plot, we

observe that the rate of change of $\gamma(t)$ and $\kappa(t)$ starts to decrease well before compression is stopped. Although $\gamma(t)$ is found to vanish much faster than $\kappa(t)$, stretching is expected to play an important role at onset. We can then anticipate that a wrinkling growth model is likely to include small but finite extensibility and bending rigidity.

We obtain the root mean square amplitude $A(t) = \sqrt{\langle w^2(x,t) \rangle}$ from the measured $w(x,t)$ to understand the growth of the buckling modes. Fig. 1(c) shows a plot of $A(t)$ as a function of time scaled with a parameter α . This parameter is chosen so that the initial growth of $A(t)$ collapses onto a single curve before a time when its rate of increase starts to decrease. Plotting α as a function of V in log-log scale in Fig. 1(d), we find that the data can be described by the function $\alpha \sim V^n$ with $n = 0.7 \pm 0.08$. This form is observed to be significantly different from a linear scaling if the dependence on time was captured simply by V .

To develop a model of this non-trivial scaling, we next consider the spatio-temporal variation of the normal deflection $w(x,t)$ and the axial strain averaged over the length given by $\gamma(t)$. We assume that axial force balance develops rapidly in our system because of the homogeneous development of wrinkles along the length of the filament in contrast with observations with very viscous fluids which show wrinkling localized near the moving ends [32]. Under these conditions, the axial tension in the filament T just depends on time and is given by $T(t) = K\gamma(t)$. Then, neglecting inertia and balancing drag, bending and stretching forces, the non-dimensional equation of evolution for $w(x,t)$ is given by

$$\dot{w} = -\frac{B}{K}\nabla^4 w + \gamma(t)\nabla^2 w. \quad (2)$$

The corresponding boundary conditions are $w(0,t) = w(1,t) = 0$, $\nabla w(0,t) = \nabla w(1,t) = 0$, $u(1,t) = 0$, and

$$u(t) \equiv u(0,t) = \begin{cases} Vt, & \text{if } t < u_f/V. \\ u_f, & \text{otherwise.} \end{cases} \quad (3)$$

We solve Eq. 2 numerically using the method of lines by discretizing the partial differential equation with finite differences in space [33]. This results in a series of ordinary differential equations (ODEs) for the evolution of the deflection. Further, differentiating the strain given in Eq. 1, an additional equation for the evolution of the strain is obtained [15]. Then, by setting the initial conditions for the deflection with white noise, the equations are integrated forward in time using the ODE solvers in MATLAB.

A sample initial spatio-temporal growth and coarsening of the wrinkles observed in the simulations by plotting $w(x,t)$ in Fig. 2(a) and $w(x,t)$ normalized by $A(t)$ in Fig. 2(b). (See supplementary documentation for a movie of the entire evolution of filament deflection till the fundamental mode is reached.) One can observe that the

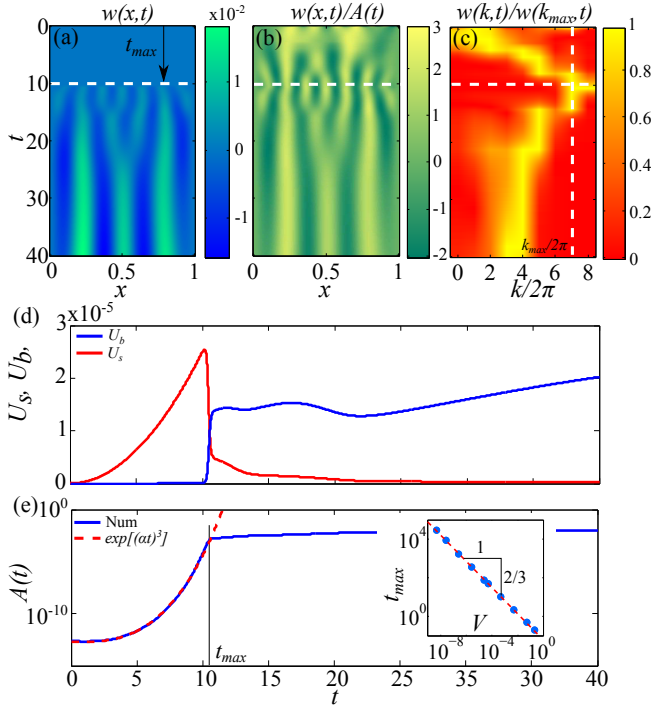


FIG. 2. (a) A map of $w(x,t)$ for $V = 5.0 \times 10^{-4}$ and $u_f = 0.1$. Compression stops at time $t_f = 200 \gg t_{max} = 10.5$. (b) Normalizing the same data as in (a) by $A(t)$ reveals the wrinkling dynamics before t_{max} . We observe an increase of the wavenumber until $t = t_{max}$ followed by a decrease. (c) Map of the Fourier mode $w(k,t)$ showing the k maximum reached at t_{max} . (d) Temporal evolution of the stretching energy U_s and the bending energy U_b shows that t_{max} is the crossover time between a stretching dominated regime (or extensible regime) and a bending dominated regime (or inextensible regime). (e) Semi-log plot of $A(t)$ shows a nonlinear growth where the amplitude can be fitted by $A_{fit}(t) = \exp(\alpha t)^3$. Inset: $t_{max} \sim 1/\alpha$ is observed to decay consistent with Eq. 8.

amplitude of the wrinkles increases rapidly and the wavelength appears to decrease till $t \approx 10$ before coarsening starts to develop and amplitude increases more slowly. To quantify the variation in wavelength, the temporal evolution of the Fourier modes as a function of k and t are plotted in Fig. 2(c). One observes that the peak in k increases initially before decreasing confirming the trends noted in the evolution of $w(x,t)/A(t)$ in Fig. 2(b). Comparing the three plots, one also observes that the rapid increase in amplitude occurs at a time similar to time t_{max} at which the wavenumber reaches a maximum $k_{max}/2\pi = 7$.

We then measure the normalized stretching energy $U_s = \frac{1}{2} \int \gamma^2(t) dx$ and bending energy $U_b = \frac{1}{2} \frac{B}{K} \int (\nabla^2 w(x,t))^2 dx$. As shown in Fig. 2(d), t_{max} is found to be the crossover time from a stretching dominated extensible regime near onset of instability to a bending dominated inextensible regime during coarsening.

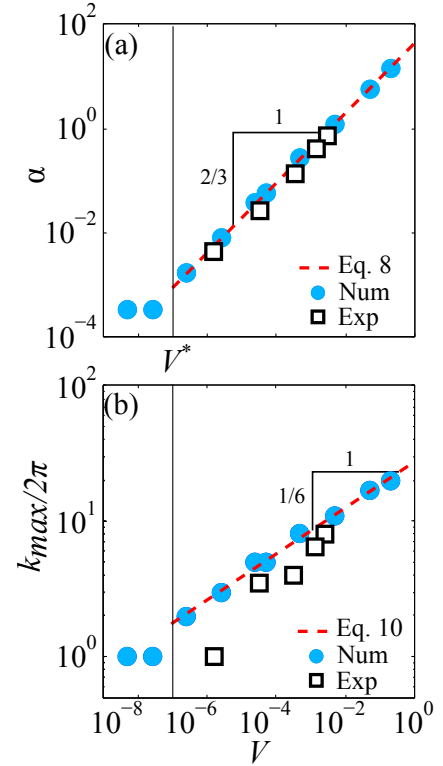


FIG. 3. The observed evolution of (a) α and (b) k_{max} with V in experiments and numerical simulation are in excellent agreement with the derived scalings in the rate-dependent loading regime above V^* indicated by a vertical line.

Fig. 2(e) shows a plot of $A(t)$ in semi-log scale which is observed to first increase faster than exponential followed by a much lower growth rate for $t > t_{max}$. We find that the initial growth is accurately fitted by $A_{fit}(t) = A_0 \exp(\alpha t)^3$ as shown in Fig. 2(e). Varying the compression speed V in the range 10^{-8} and 10^0 , we measure the dependence of t_{max} , k_{max} , and α and plot the result in Fig. 2(e)(inset), Fig. 3(a), and Fig. 3(b), respectively. Because the observed trends are captured by the dashed lines, we find that $\alpha \sim 1/t_{max} \sim V^n$ with $n = 0.68 \pm 0.05$ in very good agreement with the experiment. Further, the wavenumbers measured in the experiments and in the simulations are also in agreement with $k_{max} \sim V^{0.17}$. Thus, we conclude that the simplified Eq. 2 captures the overall evolution of the wrinkling patterns observed in the experiments. This allows us to next develop an understanding of the observed phenomena by performing a linear stability analysis around the planar undeflected configuration.

Now, Eq. 2 in Fourier space is given at linear order by

$$\dot{w}(k,t) = \left[u(t)k^2 - \frac{B}{K}k^4 \right] w(k,t), \quad (4)$$

where $w(k,t)$ is the Fourier transform of $w(x,t)$. The general solution of this equation is simply $w(k,t) = w_0 e^{\Gamma(k,t)}$ where w_0 is proportional to the amplitude of

the white noise used as initial condition in the numerics and $\Gamma(k, t) = k^2 \phi(t) - B/K k^4 t$ with $\phi(t) = \int_0^t u(t') dt'$. The standard deviation of $w(x, t)$ is then

$$A^2(t) = \frac{|w_0|^2}{2\pi} \int_{-\infty}^{+\infty} e^{2\Gamma(k, t)} dk, \quad (5)$$

where we used the Parseval-Plancherel theorem. The integral can be evaluated using the Laplace method [34]. When $\phi(t) > 0$, $\Gamma(k, t)$ reaches a maximum for $k^2 = k^{*2}(t) = K/(2B)\phi(t)/t$. Therefore,

$$A(t) \approx \frac{|w_0|/2}{\pi^{1/4}} \frac{e^{\Gamma^*(t)}}{\phi^{1/4}(t)}, \quad (6)$$

where $\Gamma^*(t) = K/(4B)\phi^2(t)/t$. Using the boundary conditions, we have $\phi(t < u_f/V) = Vt^2/2$ and $\phi(t > u_f/V) = -u_f^2/(2V) + tu_f$. Thus,

$$\Gamma^*(t) = \frac{Ku_f^2}{4B} \begin{cases} \frac{V^2 t^3}{4u_f^2}, & \text{if } t < \frac{u_f}{V} \\ \frac{u_f}{4V^2 t} - \frac{u_f}{V} + t, & \text{if } t > \frac{u_f}{V} \end{cases} \quad (7)$$

Thus, we find that $A(t) \sim \exp(\alpha t)^3$ during the loading phase is consistent with the fits used to describe the experimental and numerical data, and where

$$\alpha = \left(\frac{K}{8B} \right)^{1/3} V^{2/3}. \quad (8)$$

This calculated scaling with V is also in very good agreement with both the observed $n = 0.7 \pm 0.08$ in experiment in Fig. 1(d), and $n = 0.68$ in simulations in Fig. 2(e). Further, the fastest mode has a wavenumber

$$k^{*2}(t) \approx \frac{Vt}{4B/K}. \quad (9)$$

We cannot capture a time dependence of the wave vector near the initial growth because of the noise in the image detection, unlike $A(t)$ which is much cleaner. However, we can measure k near coarsening, i.e. when non-linearities start to dominate. These non-linearities become dominant for large amplitude occurring at a time of order $t = t_{max} \sim 1/\alpha$. Then, at time $t = t_{max}$ we have

$$k_{max}^2 = \left(\frac{K^2 V}{8B^2} \right)^{1/3}. \quad (10)$$

The derived scaling of $k_{max} \propto V^{1/6}$ is consistent with the weak $V^{0.17}$ dependence seen in the numerics and the experiment shown in Fig. 3(b) for large enough V . At the lowest V investigated, one observes that k_{max} is constant and corresponds to the fundamental mode as can be expected. The crossover speed V^* between wrinkling and buckling dynamics is derived using Eq. 10 and $k_{max} = 2\pi$ leading to $V^* \approx 8(2\pi)^6 (B/K)^2 \sim 10^{-7}$ consistent with numerical and experimental results. Thus, our analysis captures the salient features observed in our experiments and its description using Eq. 2.

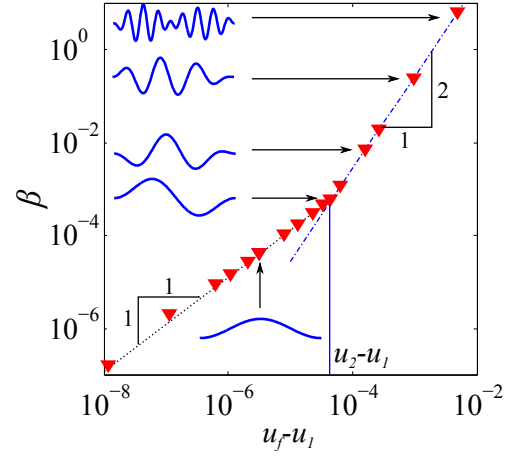


FIG. 4. Evolution of β with $u_f - u_l$ for an instantaneous compression. A crossover between a linear and quadratic trend occurs approximately at the critical compression for the first asymmetrical mode at $u_2 = 7.5 \times 10^{-5}$ yielding $u_2 - u_1 = 4.3 \times 10^{-5}$.

A widely used approximation for filament wrinkling is the sudden compression approximation obtained at large loading speed V or, equivalently, at long times ($t > u_f/V$). Using Eq. 7, we find that $A(t) \sim e^{\beta t}$ where,

$$\beta = \frac{Ku_f^2}{4B}, \quad (11)$$

and

$$k^{*2} = \frac{Ku_f}{2B}. \quad (12)$$

These results are consistent with previous linear stability analysis assuming infinite viscous medium [3] but differ when confinement is important [4, 14, 15]. While the sudden compression regime is not reached in our experiment before coarsening develops, we can examine this regime by numerically solving Eq. 2 by imposing an instantaneous compression u_f . Numerics confirms an exponential growth of the wrinkling amplitude with a growth rate β which is shown in Fig. 4 as a function of applied strain u_f . Interestingly, we find that the regime $\beta \sim u_f^2$ discussed in [3] is only valid when $u_f \gg u_1$, the strain corresponding to the buckling in the fundamental mode. Near threshold ($u_f \approx u_1$), we find another regime characterized by β linearly increasing with u_f . In this regime, the discreteness of the modes imposed by the boundary conditions plays a dominant role. When $u_1 < u_f < u_2$, the only possible wave vector is $k = 2\pi$, yielding $\dot{w}(k, t) = 4\pi^2(u_f - u_1)w(k, t)$, where $u_1 = 4\pi^2 B/K$. Upon integration, we obtain an exponential growth with a growth rate linearly depending on $u_f - u_1$ as shown in Fig. 4. However, when a sudden compression approximation is used, none of the two regimes discussed here capture the load rate dependence of the wrinkling dynamics found in our experiments.

In conclusion, our study reveals that filaments subjected to a ramped loading show a faster than exponential growth in a regime where the filament is extensible which is qualitatively different than the growth derived when assuming a sudden loading. In particular, we find the wrinkles to grow as $\exp((\alpha t)^3)$ with a timescale $\alpha^{-1} \sim \beta^{-1/3} \dot{\gamma}^{2/3}$ which is a combination of the spontaneous timescale β^{-1} of sudden compression and a timescale given by the loading rate $\dot{\gamma}$. Hence, theoretical models that examine the behavior of semi-flexible polymers and the locomotion of micro-organisms which assume rate independent loading can make a crucial overreaching approximation. Our analysis based on our model experimental system thus advances a new time scale which is important to the mechanics of filaments which are subjected to time-dependent confining stresses.

We thank Vincent Démery, Dominic Vella and Etienne Barthel for their help with the analytical and numerical analysis. This work was supported by the National Science Foundation under grant number DMR 1508186.

* julien.chopin@espci.fr

- [1] M. L. Gardel, J.H. Shin, F.C. MacKintosh, L. Mahadevan, P. Matsudaira, and D.A. Weitz, “Elastic behavior of cross-linked and bundled actin networks,” *Science* **304**, 1301 (2004).
- [2] O. Chaudhuri, S. H. Parekh, and D. A. Fletcher, “Reversible stress softening of actin networks,” *Nature* **445**, 295 (2007).
- [3] H. Jiang and J. Zhang, “Mechanics of microtubule buckling supported by cytoplasm,” *Journal of Applied Mechanics* **75**, 061019 (2008).
- [4] T. Li, “A mechanics model of microtubule buckling in living cells,” *Journal of Biomechanics* **41**, 1722 (2008).
- [5] Thomas R. Powers, “Dynamics of filaments and membranes in a viscous fluid,” *Review of Modern Physics* **82**, 1607 (2010).
- [6] Raymond E. Goldstein and Alain Goriely, “Dynamic buckling of morphoelastic filaments,” *Physical Review E: Rapid Communications* **74**, 010901 (2006).
- [7] K. Son, J.S. Guasto, and R. Stocker, “Bacteria can exploit a flagellar buckling instability to change direction,” *Nature Physics* **9**, 494 (2013).
- [8] Anke Lindner and Michael Shelley, “Elastic fibers in flows,” *RSC Soft Matter No. 1* **82**, 1607 (2012).
- [9] M. A. Biot, “Theory of folding of stratified viscoelastic media and its implications in tectonics and orogenesis,” *Geophysical Society of America Bulletin* **72**, 1595 (1961).
- [10] J. Chopin and A. Kudrolli, “Helicoids, wrinkles, and loops in twisted ribbons,” *Physical Review Letters* **111**, 174302 (2013).
- [11] J. Chopin, V. Demery, and B. Davidovitch, “Roadmap to the morphological instabilities of a stretched twisted ribbon,” *Journal of Elasticity* **119**, 137–189 (2015).
- [12] JT Miller, T Su, J Pabon, N Wicks, K Bertoldi, and PM Reis, “Buckling of a thin elastic rod inside a horizontal cylindrical constraint,” *Extreme Mechanics Letters* **3**, 36–44 (2015).
- [13] R. Vermorel, N. Vanderberghe, and E. Villermaux, “Rubber band recoil,” *Proceedings of the royal society London A* **463**, 641 (2007).
- [14] R. Huang and Z. Suo, “Wrinkling of a compressed elastic film on a viscous layer,” *Journal of Applied Physics* **91**, 1135 (2001).
- [15] Ousmane Kodio, Ian M Griffiths, and Dominic Vella, “Lubricated wrinkles: imposed constraints affect the dynamics of wrinkle coarsening,” *arXiv preprint arXiv:1609.04598* (2016).
- [16] Yoël Forterre, Jan M Skotheim, Jacques Dumais, and Lakshminarayanan Mahadevan, “How the venus flytrap snaps,” *Nature* **433**, 421–425 (2005).
- [17] Martien A Cohen Stuart, Wilhelm TS Huck, Jan Genzer, Marcus Müller, Christopher Ober, Manfred Stamm, Gleb B Sukhorukov, Igal Szleifer, Vladimir V Tsukruk, Marek Urban, *et al.*, “Emerging applications of stimuli-responsive polymer materials,” *Nature materials* **9**, 101–113 (2010).
- [18] Edwin WH Jager, Elisabeth Smela, and Olle Inganäs, “Microfabricating conjugated polymer actuators,” *Science* **290**, 1540–1545 (2000).
- [19] Yoshihito Osada, Hidenori Okuzaki, and Hirofumi Hori, “A polymer gel with electrically driven motility,” *Nature* **355**, 242–244 (1992).
- [20] Guohua Chen and Allan S Hoffman, “Graft copolymers that exhibit temperature-induced phase transitions over a wide range of ϕ ,” *Nature* **373**, 49–52 (1995).
- [21] Jungwook Kim, James A Hanna, Myunghwan Byun, Christian D Santangelo, and Ryan C Hayward, “Designing responsive buckled surfaces by halftone gel lithography,” *Science* **335**, 1201–1205 (2012).
- [22] Miguel Camacho-Lopez, Heino Finkelmann, Peter Palffy-Muhoray, and Michael Shelley, “Fast liquid-crystal elastomer swims into the dark,” *Nature Materials* **3**, 307–310 (2004).
- [23] Casper L van Oosten, Cees WM Bastiaansen, and Dirk J Broer, “Printed artificial cilia from liquid-crystal network actuators modularly driven by light,” *Nature Materials* **8**, 677–682 (2009).
- [24] Yanlei Yu, Makoto Nakano, and Tomiki Ikeda, “Photomechanics: directed bending of a polymer film by light,” *Nature* **425**, 145–145 (2003).
- [25] JR Gladden, NZ Handzy, Andrew Belmonte, and Emmanuel Villermaux, “Dynamic buckling and fragmentation in brittle rods,” *Physical Review Letters* **94**, 035503 (2005).
- [26] C.P. Brangwynne, G.H. Koenderink, E. Barry, Z. Dogic, F.C. MacKintosh, and David A. Weitz, “Bending dynamics of fluctuating biopolymers probed by automated high-resolution filament tracking,” *Biophysical Journal* **93**, 346 (2007).
- [27] Chris H Wiggins, D Rivelin, Albrecht Ott, and Raymond E Goldstein, “Trapping and wiggling: elastohydrodynamics of driven microfilaments,” *Biophysical Journal* **74**, 1043–1060 (1998).
- [28] GK Batchelor, “Slender-body theory for particles of arbitrary cross-section in stokes flow,” *Journal of Fluid Mechanics* **44**, 419–440 (1970).
- [29] Thomas R Powers, “Dynamics of filaments and membranes in a viscous fluid,” *Reviews of Modern Physics* **82**, 1607 (2010).
- [30] Lev Davidovich Landau and Eugin M Lifshitz, *Course of theoretical physics, Theory of elasticity* (Pergamon Press

- Oxford, 1986).
- [31] See Supplementary Documentation for a movie of the shape evolution, the calculation of the Euler buckling modes, and the comparison of the fundamental mode with the final shape shown of the filament.
 - [32] F. P. Gosselin, P. Neetzow, and M. Paak, “Buckling of a beam extruded into highly viscous fluid,” *Physical Review E* **90**, 052718 (2014).
 - [33] Alain Vande Wouwer, Philippe Saucez, Carlos Vilas, *et al.*, *Simulation of ODE/PDE Models with MATLAB, OCTAVE and SCILAB* (Springer, 2014).
 - [34] Chris J Budd and Mark A Peletier, “Approximate self-similarity in models of geological folding,” *SIAM Journal on Applied Mathematics* **60**, 990–1016 (2000).
- Author Contributions:** J.C. and A.K. designed the research; J.C and M.D. performed the experiments; J.C. developed the numerical model; J.C., M.D. and A.K. analyzed data; and J.C. and A.K. wrote the paper.